Systematic Analysis of RF Distortion in SiGe HBT's

Guofu Niu, Qingqing Liang, John D. Cressler, Charles S. Webster[1], and David L. Harame[1]

ECE Department, 200 Broun Hall, Auburn University, Auburn, AL 36849, USA
Tel: 334 844-1856 / Fax: 334 844-1888 / E-mail: guofu@eng.auburn.edu
[1]IBM Microelectronics, Essex Junction, VT 05452, USA

I. Introduction

RF circuits often require highly linear transistors with very low intermodulation distortion. Intermodulation measurement in the GHz range requires substantial effort, and is very time consuming, making modeling attractive. The classical approach to modeling distortion is to use transient analysis followed by Fourier transform or harmonic balance. These methods compute the circuit response by iteration, resulting in a list of numbers that do not indicate which physical nonlinearities are limiting the overall linearity. Such information, however, can be obtained using Volterra series [1]–[3]. The price for the extra insight is that the analysis is only applicable to RF circuits with small input power.

Fortunately, many RF amplifiers in mobile communication circuits operate at relatively small input power, including low-noise amplifiers (LNA), making Volterra series applicable. This work presents the first systematic analysis of RF intermodulation in SiGe HBT's using a Volterra series-based new approach. Our goal is to identify the linearity limiting factors at the device level in a SiGe HBT RF technology [4], and to explore the physics underlying the load dependence that is of great importance for circuit design. In particular, we examine the impact of avalanche multiplication, which has been a concern for SiGe HBTs because of their inherently low breakdown voltage. The results show that the negative impact of avalanche multiplication can be substantially alleviated by proper choice of biasing current. The impact of collector profile design, and its implications to RF IC design are also discussed. Details of the UHV/CVD SiGe HBT technology used can be found in [4].

II. Transistor Modeling

Distortion analysis demands accurate modeling of transistor I-V and C-V characteristics. Fig. 3 depicts the equivalent circuit used in this work and includes the dominant nonlinearities. I_{CE} represents the collector current transported from the emitter, I_{BE} represents the hole injection into the emitter, I_{CB} represents the avalanche multiplication current:

$$\begin{aligned} I_{CB} &= I_{CE}(M-1) \\ &= I_{C0}(V_{BE})F_{Early}(M-1) \end{aligned} \quad (1)$$

where $I_{C0}(V_{BE})$ is the I_C measured at zero V_{CB}, M is the avalanche multiplication factor, and F_{Early} is the Early effect factor [6]. The elements values were extracted using measured DC data and S-parameters up to 40GHz. To suppress Kirk effect, the collector is doped as high as $10^{18}/cm^3$ in high speed SiGe HBTs. This results in high avalanche multiplication (M-1) and low breakdown voltage. M-1 is often modeled only as a function of V_{CB}. In the SiGe HBTs used in this work, M-1 is also a strong function of the collector current density J_C. We first attempted to apply the M-1 model proposed in [5], but could not get satisfactory fitting to the measured M-1 for the SiGe HBTs under investigation. A new equation was then developed to describe the V_{CB} and J_C dependence of M-1:

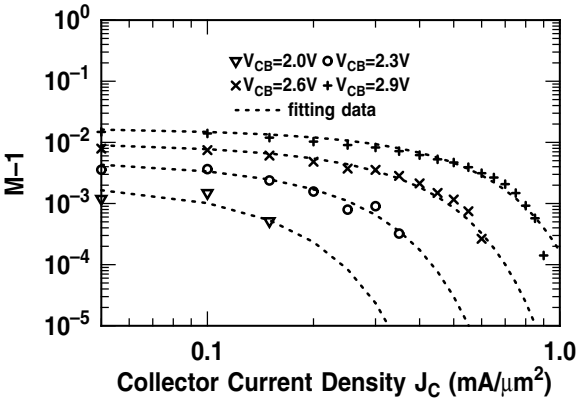

Fig. 1. Comparison of the measured and modeled avalanche multiplication factor (M-1) as a function of J_C for different V_{CB}.

$$M-1 = \frac{V_{CB}}{\alpha V_{CBO}} \exp\left(-\frac{m\alpha^{-1/3}}{V_{CB}^{2/3}}\right) \quad (2)$$

$$\alpha = 1 - \tanh\left[\frac{I_C}{I_{CO}} \exp\left(\frac{V_{CB}}{V_R}\right)\right] \quad (3)$$

where m, V_{CBO}, I_{CO}, and V_R are fitting parameters.

Fig. 1 shows the fitting of the measured M-1 data as a function of J_C using the proposed M-1 equation. Physically, M-1 decreases with increasing collector current density J_C because of the compensation of the depletion charge (qN_D) by the mobile carrier ($-J_c/v$). This effectively reduces the net charge density and hence the electric field in the CB junction. At sufficiently high J_C, the net charge density reduces to zero, and base push-out occurs, resulting in the roll-off of f_T. Fig. 2 shows the measured f_T and f_{max} vs J_C on the same device as in Fig. 1. Note that M-1 starts to decrease at a J_C value that is much smaller than the J_C where we reach peak f_T and f_{max}.

III. Circuit Analysis

A single transistor amplifier was used (Fig. 4). The nonlinear circuit was first linearized, and solved:

$$Y(s) \cdot \vec{H}_1(s) = \vec{I}_1 \quad (4)$$

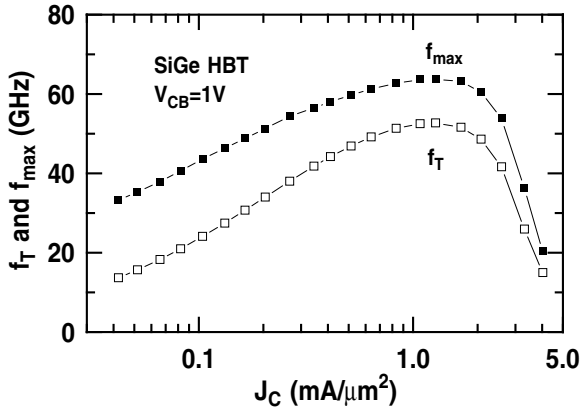

Fig. 2. Measured f_T and f_{max} as a function of J_C for the SiGe HBTs used in this work.

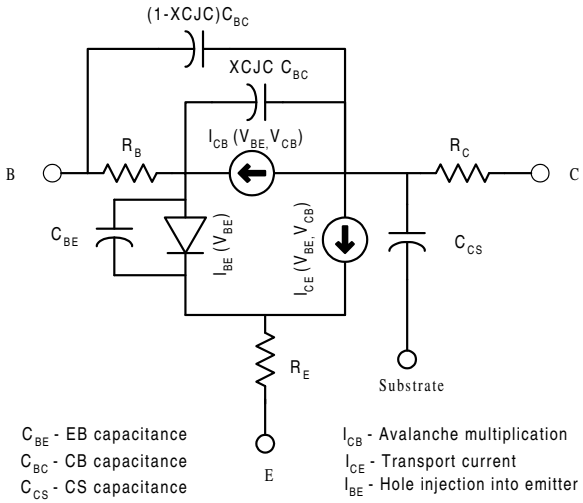

Fig. 3. Equivalent circuit of the SiGe HBT used for Volterra series simulations.

where $Y(s)$ is the CMNA [7] admittance matrix at frequency s, $\vec{H}_1(s)$ is the vector of first-order Volterra kernel transforms of the node voltages, and $\vec{I}_1$ is the vector of excitations.

With $\vec{H}_1(s)$ solved, the same circuit was excited by the second-order nonlinear current sources $\vec{I}_2$, which were determined by the first order voltages that control individual nonlinearities, and the second-order derivatives of all the $I-V$ and $C-V$ nonlinearities. The node voltages under such an excitation are the second-order Volterra kernels $\vec{H}_2(s_1, s_2)$:

$$Y(s_1 + s_2) \cdot \vec{H}_2(s_1, s_2) = \vec{I}_2 \tag{5}$$

where $Y(s_1 + s_2)$ is the same CMNA admittance matrix used in Eq. (4), but evaluated at the frequency $s_1 + s_2$.

In a similar manner, the third-order Volterra kernels $\vec{H}_3$ were solved as response to excitations specified in terms of the previously determined first and second-order kernels:

$$Y(s_1 + s_2 + s_3) \cdot \vec{H}_2(s_1, s_2, s_3) = \vec{I}_3 \tag{6}$$

P_{out} vs P_{in}, the 3rd order input intercept (IIP3) at which the 1st and 3rd order signals have equal power, and the (power) gain can then be obtained from $\vec{H}_3$ and $\vec{H}_1$.

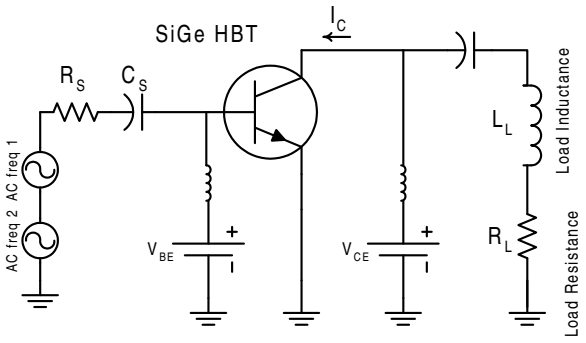

Fig. 4. Circuit schematic of the single transistor amplifier used.

IV. Identifying Dominant Nonlinearity

One of the major advantage of the Volterra series approach is the ability to identify the dominant nonlinearity [2]. The identification is traditionally realized by separating $\vec{H}_3$ into several components related to each individual nonlinearity [2]. The overall $\vec{H}_3$ is simply the sum of the individual $\vec{H}_3$. This, however, does not completely distinguish individual nonlinearities because the solution of $\vec{H}_2$ involves all the nonlinearities, and $\vec{H}_2$ was used in the calculation of $\vec{I}_3$.

To completely distinguish individual nonlinearities, we propose here a new approach. For each nonlinearity, both $\vec{H}_2$ and $\vec{H}_3$ are solved using *only* the virtual current source excitation related to the specific nonlinearity in question. An individual IIP3 is thus obtained for each nonlinearity. The individual nonlinearity that gives the lowest IIP3 (the worst linearity) is identified as the dominant nonlinearity.

We then calculate the overall IIP3 by including all of the nonlinearities in the calculation of both $\vec{H}_2$ and $\vec{H}_3$. A comparison of the individual IIP3 and the overall IIP3 reveals the interaction between individual nonlinearities. As shown later, the overall IIP3 obtained by including all of the nonlinearities can be larger (better) than an individual IIP3, implying cancellation between individual nonlinearities. Unlike in the traditional approach, the overall $\vec{H}_3$ is not equal to the sum of all of the individual $\vec{H}_3$, because of the complete separation of individual nonlinearities.

V. Results and Discussion

A. Comparison with Measurement

Volterra series is only applicable to low input power, such as the signal levels at a mobile receiver (as low as -100 dBm). IIP3 measurements, however, are often made at much higher P_{in} to improve measurement accuracy. Volterra series is less accurate for these measurement conditions. Nevertheless, a comparison with measurement still provides a test of the accuracy of the simulation, and is shown in Fig. 5. The agreement with measurement is excellent for the fundamental signal, and is within 5dB for the intermodulation signal at $P_{in} = -30dBm$. This is acceptable considering that -30 dBm is "large" for the small-signal distortion requirement.

B. Bias Current and Voltage Dependence

Fig. 6 shows IIP3 and gain as a function of I_C up to 60mA at which f_T and f_{max} peak. At very low I_C (<5mA), the exponential $I_{CE} - V_{BE}$ nonlinearity (×) yields the lowest individual IIP3, and

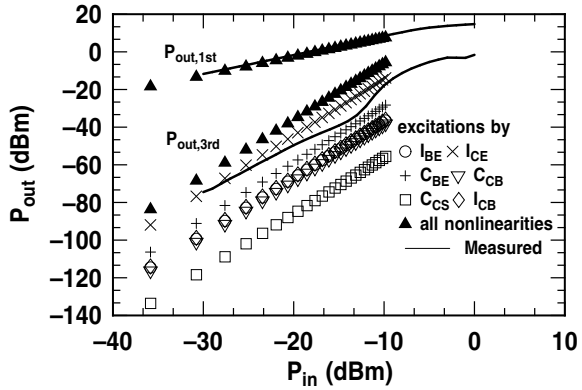

Fig. 5. Comparison of the simulated and measured P_{out} versus P_{in} at 2GHz for a single transistor SiGe HBT amplifier. $A_E = 0.5 \times 20 \times 4\mu m^2$. $I_C = 3mA, V_{CE} = 3V$, $R_S = 50\Omega, C_S = 300pF, R_L = 186\Omega, L_L = 9nH$. Tone spacing is 1MHz.

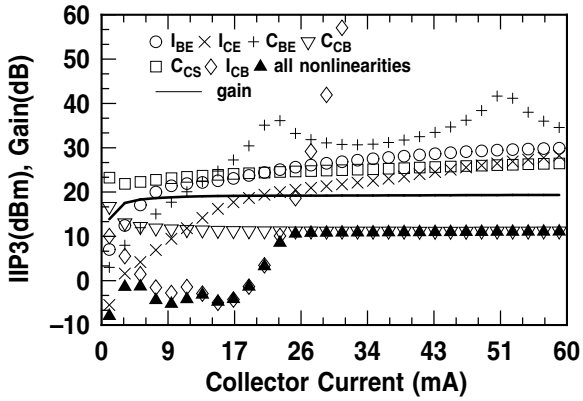

Fig. 6. IIP3 and gain as a function of I_C.

hence is the dominant factor. For $5mA < I_C < 25mA$, the I_{CB} nonlinearity due to avalanche multiplication ($\diamond$) dominates. For $I_C > 25mA$, the C_{CB} nonlinearity due to the CB capacitance ($\triangledown$) dominates. Interestingly, the overall IIP3 obtained by including all of the nonlinearities is close to the lowest individual IIP3 for all the I_C. The closeness indicates that the interaction between individual nonlinearities is weak.

The overall IIP3 increases with I_C for $I_C < 5mA$ when the exponential I_{CE} nonlinearity dominates. For $I_C > 5mA$ where the avalanche current (I_{CB}) nonlinearity dominates, the I_C dependence of the overall IIP3 is twofold:

1. The initial current for avalanche I_{CE} increases with I_C.
2. The avalanche multiplication factor (M-1) decreases with I_C.

Even though the details of the simulated overall IIP3 curve cannot be easily explained, the increase of the avalanche IIP3 and hence the overall IIP3 for $I_C > 17mA$ can be readily understood as a result of the decrease of M-1 with increasing J_C. For $I_C > 25mA$, the overall IIP3 is limited by the C_{CB} nonlinearity, and is approximately a constant. The optimum biasing current is therefore $I_C = 25mA$. The use of a higher I_C only increases power consumption. The decrease of M-1 with increasing J_C is therefore beneficial to the linearity of these SiGe HBTs. To our knowledge, this is the only beneficial effect of the charge compensation by mobile carriers in the CB junction space charge region. Our simulation results also indicate the importance of modeling the J_C dependence of M-1.

To minimize noise, low-noise amplifiers in this technology are typically biased at a J_C of 0.1-0.2$mA/\mu m^2$, which corresponds to a I_C of 4-8mA in Fig. 6. In this bias range, IIP3 is limited by avalanche multiplication. For further improvement of IIP3, a lower collector doping is desired, provided that the noise performance is not inadvertently degraded. Our earlier work showed that the noise figure is relatively independent of the collector doping as long as Kirk effect does not occur at the J_C of interest [9]. Thus, there must exist an optimum collector doping profile for producing low noise transistors with the best linearity.

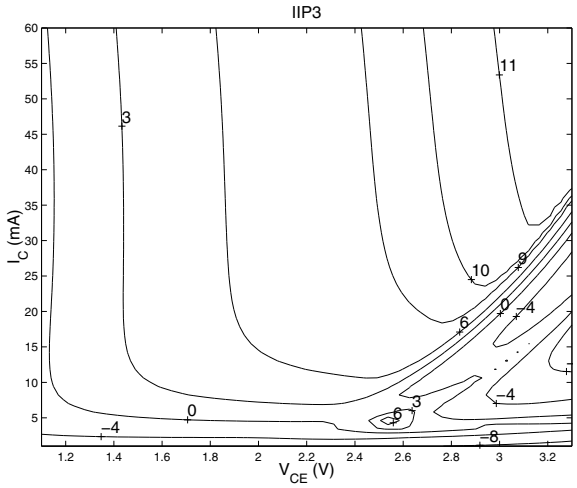

Fig. 7. Contours of IIP3 in dBm on the $I_C - V_{CE}$ plane.

C. Load Dependence and Cancellation Between C_{CB} and I_{CB} Nonlinearities

Experimentally, it is well established that linearity depends on the circuit load. Fig. 8 shows the IIP3 simulated with individual and all nonlinearities vs load resistance. Gain varies with load, and peaks when the load is closest to conjugate matching, as expected. IIP3, however, is much more sensitive to load variation.

The IIP3 with all nonlinearities (denoted by ▲) is noticeably higher than the IIP3 with the avalanche current (I_{CB}) nonlinearity alone (denoted by $\diamond$). The interaction between individual nonlinearities has improved the overall linearity through cancellation. In this case, the two most dominating nonlinearities are the avalanche current I_{CB} nonlinearity and the C_{CB} nonlinearity. The cancellation between the I_{CB} and C_{CB} nonlinearities leads to an overall IIP3 values that is higher (better) than the IIP3 obtained using the I_{CB} nonlinearity alone. The degree of cancellation depends on the biasing, source and load conditions, as expected from the Volterra series theory. The cancellation between the I_{CE} and C_{BE} analyzed in [8] is not important here.

We attribute the load dependence of linearity in these HBTs to the CB feedback due to the avalanche current I_{CB} and the CB capacitance C_{CB}. For verification, the simulation was repeated by setting $C_{CB} = 0$ and $I_{CB} = 0$. The experimentally extracted F_{Early} and R_E were used. The results in Fig. 9 support our speculation. IIP3 becomes virtually independent of load for all of the nonlinearities except for the C_{CS} nonlinearity. The individual IIP3 due to C_{CS} depends on the load, because the load directly affects

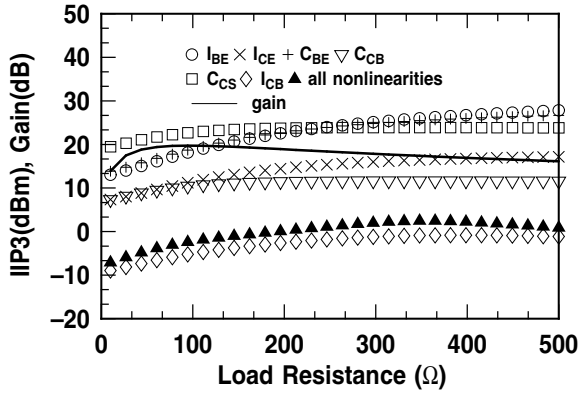

Fig. 8. IIP3 and gain as a function of load resistance at $I_C = 13mA$.

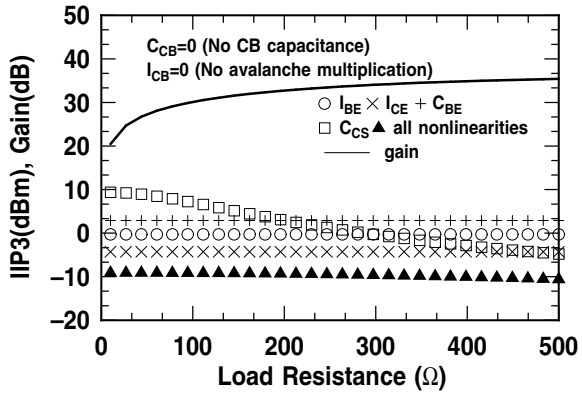

Fig. 9. IIP3 and gain vs load resistance at $I_C = 13mA$. $C_{CB} = 0$ and $I_{CB} = 0$.

the controlling voltage of the C_{CS} nonlinearity. This, however, virtually has no effect on the load dependence of the overall linearity because C_{CS} is not important for the overall nonlinearity.

D. Linearity Limiting Factors

Fig. 10 shows the dominant nonlinearity factor on the $I_C - V_{CE}$ plane. The source and load conditions are the same as in Fig. 5. However, the results obtained using other load conditions are similar. The upper limit of I_C is where f_T reaches its peak value. Avalanche multiplication and C_{CB} nonlinearities are the dominant factors for most of the bias currents and voltages. From device physics, both avalanche multiplication and C_{CB} nonlinearities can be reduced by reducing the collector doping. This conflicts with the need for high collector doping to suppress Kirk effect and heterojunction barrier effects in SiGe HBTs. This suggests that multiple collector doping profiles are needed to provide both high f_T devices and high IIP3 devices for different stages of the same circuit. In processing, this can be achieved by selective ion implantation.

VI. Summary

A systematic analysis of the RF intermodulation in SiGe HBT's is performed using a new Volterra series-based approach. The relative dominance of individual nonlinearities and their interaction were shown to vary with source/load, bias current, and CB feedback. The C_{CB} and avalanche multiplication nonlinearities are the dominant factors in determining the overall linearity, and are responsible for the load dependence. A cancellation mechanism between the avalanche current I_{CB} nonlinearity and the CB capacitance C_{CB} nonlinearity is identified. The current dependence of avalanche multiplication was shown to be beneficial to linearity. The results suggest that there is a fundamental limit to achieving high f_T and high linearity, and multiple collector profiles need to be used for leverage in RF circuit design.

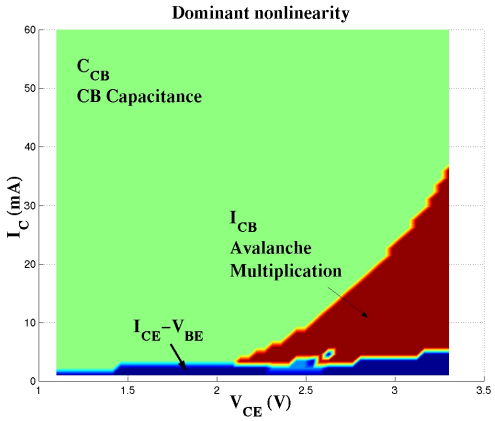

Fig. 10. Dominant nonlinearity factor on the I_C - V_{CE} plane.

Acknowledgments

This work was supported by an IBM University Partner Award, and SRC under # 2000-HJ-769. The wafers were fabricated at IBM Microelectronics, Essex Junction, VT. We would like to thank D. Ahlgren, S. Subbanna, N. King, W. Ansley, A.J. Joseph, S. Taylor, and B. Meyerson for their contributions.

References

[1] V. Volterra, *Theory of Functionals and of Integral and Integro-Differential Equations*, Dover, 1959.
[2] P. Wambacq and W. Sansen, *Distortion Analysis of Analog Integrated Circuits*, Kluwer Academic, 1998.
[3] S. Narayanan, *Bell System Technical Journal*, vol. 46, no. 3, pp. 991-1024, May-June 1967.
[4] D.C. Ahlgren et al., *Tech. Dig. IEDM*, pp. 859-862, 1996.
[5] W.J. Kloosterman et al., *Proc. IEEE BCTM*, pp. 172-175, 2000.
[6] G.F. Niu et al., *IEEE Trans. Electron Devices*, vol. 46, no. 5, pp. 1007-1015, May 1999.
[7] G. Gielen, and W. Sansen, *Symbolic Analysis for Automated Design of Analog Integrated Circuits*, Kluwer Academic, 1991.
[8] S. Maas et al., *IEEE Trans. Microwave Theory and Techniques*, vol. 40, no. 3, pp. 442-448, March 1992.
[9] G.F. Niu et al., *IEEE Trans. Electron Devices*, vol. 46, no. 8, pp. 1347-1354, Aug. 1999.